A Preliminary Polarimetric Radar Comparison of Pretornadic and Nontornadic Supercell Storms

MATTHEW S. VAN DEN BROEKE

Department of Earth and Atmospheric Sciences, University of Nebraska–Lincoln, Lincoln, Nebraska

(Manuscript received 4 September 2019, in final form 31 January 2020)

ABSTRACT

Supercell thunderstorms produce a variety of hazards, including tornadoes. A supercell will often exist for some time prior to producing a tornado, while other supercells never become tornadic. In this study, a series of hypotheses is tested regarding the ability of S-band polarimetric radar fields to distinguish pretornadic from nontornadic supercell storms. Several quantified polarimetric radar metrics are examined that are related to storm inflow, updraft, and hailfall characteristics in samples of 19–30 pretornadic and 18–31 nontornadic supercells. The results indicate that pretornadic supercells are characterized by smaller hail extent and echo appendages with larger mean drop size. Additionally, differential reflectivity Z_{DR} column size is larger and less variable in the pretornadic storms in the 25–30 min prior to initial tornadogenesis. Many of the results indicate relatively small polarimetric differences that will likely be difficult to translate to operational use. Hail extent and Z_{DR} column size, however, may exhibit operationally useful differences between pretornadic and nontornadic supercells.

1. Introduction

Typical polarimetric radar features of supercell storms are well known in the literature (Kumjian and Ryzhkov 2008a; Romine et al. 2008; Van Den Broeke et al. 2008; Kumjian et al. 2010; French et al. 2015; Tanamachi and Heinselman 2016; Van Den Broeke 2016; and many others). One recent focus has been to quantify these features (e.g., Kumjian 2011; Snyder et al. 2015; Van Den Broeke 2016) and apply them across the tornado life cycle (e.g., French et al. 2015; Houser et al. 2016; Van Den Broeke 2017). Fewer studies have quantified how tornadic and nontornadic supercell storms may differ polarimetrically (e.g., French et al. 2015). Kumjian and Ryzhkov (2007) examined a sample of nine tornadic and six nontornadic supercell storms and found generally similar and repeatable polarimetric signatures across the sample, though their primary purpose was not to examine differences between tornadic and nontornadic storms. Here the results of a study are reported that seek to separate nontornadic and pretornadic supercell storms using their polarimetric radar characteristics.

An overview of the tornado warning process including current challenges is provided by Brotzge and Donner (2013). One challenge in identifying potentially tornadic storms is that they occasionally occur in such close proximity to nontornadic storms that the observational network is unable to distinguish their environments (e.g., Klees et al. 2016). In this case, radar signatures may be critically important to determine the tornadic potential of individual storms. Severe weather predictability can be extremely sensitive to mesoscale details (e.g., Bluestein and Snyder 2015), and thus any attempt to use radar information for this purpose must be supplemented by available knowledge of the regional- and storm-scale environment. The reader is referred to Klees et al. (2016) for a review of the primary documented kinematic and nonpolarimetric radar differences between tornadic and nontornadic supercell storms.

The radar-observed hook echo or echo appendage (e.g., Stout and Huff 1953; Forbes 1981; Markowski 2002) has been associated with tornadic thunderstorms since the early days of radar meteorology but is not a reliable predictor of tornadic potential (e.g., Forbes 1981; Markowski et al. 2002). Nevertheless, properties of the drop size distribution within the appendage may be a predictor of whether a storm is tornadic. Tornadic appendages have been associated with greater areal predominance of small drops (Kumjian and Ryzhkov 2008b), and small drops may become more numerous in the appendage prior to tornadogenesis (French et al. 2015).

Corresponding author: Matthew S. Van Den Broeke, mvandenbroeke2@unl.edu

DOI: 10.1175/MWR-D-19-0296.1

Cao et al. (2008, hereafter C08) developed a curve to be placed on a scatterplot of radar reflectivity (Z_{HH}) and differential reflectivity (Z_{DR}) characterizing "typical" rainfall in Oklahoma, which can be used to determine whether median drop size is larger than expected for Oklahoma rainfall (points above the C08 curve) or smaller than expected (points below the C08 curve). Prior work has found that tornadic supercells are more likely than nontornadic supercells to have a larger proportion of appendage points lying below the C08 curve (French et al. 2015), indicating relatively small median drop size.

Environmental characteristics show some skill in determining whether supercells will be tornadic or nontornadic (e.g., Stensrud et al. 1997; Thompson 1998; Coffer and Parker 2017). Tornadic and nontornadic environments are somewhat distinguished by observations of environmental characteristics (e.g., Brooks et al. 1994; Rasmussen and Blanchard 1998; Rasmussen 2003; Thompson et al. 2003; Davies 2004; Esterheld and Giuliano 2008; Mercer et al. 2009; Parker 2014; Klees et al. 2016; and others). For example, prior work has shown that high values of boundary layer–6 km shear reasonably distinguish supercells from nonsupercells, but this quantity does not skillfully distinguish significantly tornadic supercells (those producing tornadoes rated EF2+) from weakly tornadic and nontornadic supercells (Rasmussen and Blanchard 1998; Thompson et al. 2003). Storm relative helicity (SRH) and low-level shear are shown to better distinguish tornadic from nontornadic supercells. The greater applicability of 0–1 and 0–3 km products [e.g., SRH, convective available potential energy (CAPE)] was discussed and quantified by Rasmussen (2003), and mixed-layer parameters were examined by Thompson et al. (2003). Many of these parameters may have operationally meaningful ability to distinguish tornadic from nontornadic environments (e.g., Klees et al. 2016) if the observational network takes samples at sufficient resolution. The high-resolution dataset of Parker (2014) indicates that tornadic supercell environments are distinguished by higher low-level mixing ratio values and a more strongly veering wind profile in the lowest 1 km.

Such environmental differences may translate to differences in supercell inflow, updraft, and microphysical characteristics, in turn leading to variable manifestations of supercell polarimetric features (e.g., French et al. 2015; Van Den Broeke 2016). Since these differences are closely tied to the environment, nontornadic supercells may exhibit different polarimetric characteristics than supercells, which will eventually produce a tornado. If this is the case, polarimetric information may be helpful to determine which storms are most likely to become tornadic in the near future. So far, however, little work has quantified polarimetric signatures and their differences within samples of pretornadic and nontornadic supercells to examine whether these supercell populations may be distinguishable. The goal of this paper is to test several hypothesized differences between nontornadic and pretornadic supercell storms in the 15–30 min prior to initial tornadogenesis, described below:

1) Hailfall may display greater temporal variability in tornadic supercells than in nontornadic supercells (e.g., Kumjian and Ryzhkov 2008a, 2009; Van Den Broeke 2016). Therefore, pretornadic supercells in this study are hypothesized to be distinguished by a hail signature that exhibits greater temporal variability in size. A higher proportion of analysis periods with relatively small hail extent is also hypothesized to result in smaller median storm-core Z_{HH} values in pretornadic supercells compared to nontornadic supercells.
2) Nontornadic supercells often exhibit consistent and pronounced Z_{DR} arc disruptions due to hailfall, which is more extensive spatially and temporally than in tornadic supercells (e.g., Kumjian and Ryzhkov 2009). Thus, for this study pretornadic storms are hypothesized to have steadier Z_{DR} arc characteristics (width, size, and Z_{DR} value within the arc) when a larger sample is examined due to less frequent hailfall disruptions.
3) Given a smaller contribution from melting hail (e.g., as hypothesized by Dawson et al. 2014) and consistent with the findings of Van Den Broeke (2017) for times when a supercell was producing a tornado, the Z_{DR} arcs of pretornadic supercells are hypothesized to contain higher median Z_{DR} values than are nontornadic supercells.
4) Past numerical studies have indicated a possible but likely relatively weak positive association between low-level vortex intensity and midlevel updraft size for mesocyclone-associated tornadoes (e.g., Trapp et al. 2017; Coffer and Markowski 2018). Radar-based evidence for a possible relationship between vortex intensity and midlevel updraft size, depth, and steadiness was presented by Van Den Broeke (2016, 2017). Thus, updrafts are hypothesized to be larger, deeper, and steadier in pretornadic supercells than in nontornadic supercells, though such associations may be weakened by the relatively poor vertical resolution of operational radar data.
5) Echo appendages of tornadic storms may on average contain smaller drops than nontornadic storms (e.g., Kumjian and Ryzhkov 2008b; French et al. 2015), though this varies by location within the appendage

TABLE 1. The date, analysis period, representative radar, and unanalyzed metrics for the 32 pretornadic supercell storms included in this study. The unanalyzed metric numbers follow the metric descriptions in section 2 of this paper.

Date of supercell	Analysis period (UTC)	Radar	Metrics not analyzed
26 Apr 2012	2337–0000	KOHX	
30 Apr 2012	2229–2257	KDDC	
10 May 2012	1819–1847	KEWX	6
9 Jun 2012	0001–0030	KMQT	
18 Mar 2013	2140–2208	KFFC	
31 Mar 2013	0207–0235	KINX	
31 Mar 2013	0353–0419	KSRX	1, 2, 3, 4, 5, 8, 9, 10, 11
17 Apr 2013	2322–2347	KFDR	
5 May 2013	0045–0115	KJAX	
15–16 May 2013	2337–0002	KFWS	8, 9, 10, 11
18–19 May 2013	2351–0014	KDDC	8, 9, 10, 11
19 May 2013	2054–2119	KTLX	
20 May 2013	2030–2056	KINX	
20 May 2013	2128–2156	KEAX	8, 9, 10, 11
31 May 2013	0025–0052	KINX	
18 Jun 2013	2204–2230	KRAX	
19 Jun 2013	2216–2245	KLBB	
28 Aug 2013	0433–0450	KDTX	
31 Aug–1 Sep 2013	2349–0010	KBIS	
11 May 2014	1956–2026	KUEX	6, 7, 8, 9, 10, 11
9 Apr 2015	2138–2200	KDVN	3, 4, 5, 8, 9, 10, 11
27 Apr 2015	0141–0205	KFWS	8, 9, 10, 11
8 May 2015	2054–2121	KFDR	8, 9, 10, 11
19 May 2015	1915–1936	KTLX	
27 May 2015	1933–1958	KDDC	8, 9, 10, 11
4 Jun 2015	2211–2237	KFTG	
22–23 Jun 2015	2347–0013	KDVN	8, 9, 10, 11
18 Sep 2015	2243–2309	KEAX	
2 Feb 2016	2021–2047	KDGX	2, 3, 4, 5, 6, 8, 9, 10, 11
24 Feb 2016	2035–2100	KRAX	4, 8, 9, 10, 11
29 Apr 2016	1959–2025	KFDR	8, 9, 10, 11
21 Oct 2017	2156–2220	KFDR	7

(French et al. 2015). If greater prevalence of melting hail in the appendages of nontornadic storms is responsible as speculated prior (Kumjian and Ryzhkov 2008b), it is here hypothesized that nontornadic appendages will be characterized by higher median Z_{HH} and Z_{DR} values, lower median ρ_{hv}, and a higher portion of bins falling above the C08 curve, consistent with larger drops and the presence of mixed-phase precipitation.

This study also provides guidance about which polarimetric radar characteristics may, with further work, be used to operationally diagnose storms with higher tornadic potential, and may provide insight into possible structural and microphysical differences between pretornadic and nontornadic supercell storms.

2. Data and methods

Samples of 32 pretornadic and 31 nontornadic supercell storms were compared in this study, though for individual radar metrics the number of contributing storms was lower as noted below. The sample of pretornadic storms is described in Table 1. The time of the first tornado report was determined for each of these supercells, and all radar scans beginning ≤30 min prior were defined as pretornado times. To be included in the analysis, the base-scan radar beam centerline throughout the polarimetric signature of interest was required to be ≤1 km above radar level (ARL; assuming beam propagation in a standard atmosphere). This resulted in five–eight sample volumes for each pretornadic supercell. These were further categorized as being 30, 25, 20, and/or 15 min prior to initial tornadogenesis, and separate analyses were conducted for each temporal length to examine whether there may be an optimal length of time prior to tornadogenesis when particular radar metrics are especially able to indicate future tornado potential.

A sample of 31 completely separate nontornadic supercell storms (Table 2) was developed following a similar method, by searching for storms containing radar

TABLE 2. As in Table 1, but for the 31 nontornadic supercell storms included in this study.

Date of supercell	Analysis period (UTC)	Radar	Metrics not analyzed
30 Apr 2012	0429–0543	KAMA	
1 Jun 2012	2334–2359	KAMA	1, 2, 3, 4, 5, 8, 9, 10, 11
10 Mar 2013	0204–0250	KEWX	1, 2, 3, 4, 5, 8, 9, 10, 11
18 Mar 2013	2004–2100	KDGX	1, 2, 3, 4, 5, 8, 9, 10, 11
2 Apr 2013	2001–2112	KGRK	1, 2, 3, 4, 5, 8, 9, 10, 11
7–8 Apr 2013	2315–0032	KSGF	
22–23 Apr 2013	2326–0003	KVNX	
22–23 Apr 2013	2347–0039	KVNX	8, 9, 10, 11
27 Apr 2013	0102–0201	KTLX	
27 Apr 2013	0210–0257	KTLX	8, 9, 10, 11
21 May 2013	0133–0157	KDMX	3, 4, 5, 8, 9, 10, 11
25 May 2013	2103–2159	KUDX	
30 May 2013	1815–1900	KTLX	
30 May 2013	1842–1933	KTLX	1, 8, 9, 10, 11
13–14 Jun 2013	2318–0033	KBLX	3, 4, 5
17 Jun 2013	1932–2036	KDTX	
4–5 Jul 2013	2304–0023	KJKL	
9–10 Jul 2013	2326–0011	KABR	
22 Jul 2013	0306–0339	KMVX	1, 2, 3, 4, 5, 8, 9, 10, 11
23 Jul 2013	2009–2058	KUDX	8, 9, 10, 11
25 Jul 2013	0002–0027	KUEX	1, 2, 3, 4, 5, 8, 9, 10, 11
6 Aug 2013	2304–2359	KMPX	
13 Aug 2013	1223–1305	KDIX	
14–15 Aug 2013	2339–0043	KAMA	
14 Oct 2013	1939–2025	KDDC	8, 9, 10, 11
27 Oct 2013	0003–0110	KFWS	
3 Apr 2014	0210–0344	KICT	
24 Apr 2014	0012–0147	KDYX	1, 2, 3, 4, 5, 8, 9, 10, 11
20 May 2014	2110–2157	KFTG	
21 May 2014	0131–0216	KLOT	
4 Sep 2014	0523–0619	KBIS	

features described by Thompson et al. (2003) within 100 km of a polarimetric Weather Surveillance Radar-1988 Doppler (WSR-88D) and not connected to other convective cells with $Z_{HH} > 20$ dBZ. Storms were selected that had base-scan data ≤1 km ARL for ≥20 min so reasonably robust time series of low-level radar metrics could be developed. Analysis periods ranged in length from 24 min to 1 h 45 min, with an average length of 56 min. As with the sample of pretornadic storms, events were chosen without regard to geographic region (Fig. 1) or time of year (Tables 1 and 2). Events were classified as nontornadic if the Storm Events Database (https://www.ncdc.noaa.gov/stormevents/) from the National Centers for Environmental Information (NCEI) indicated that no tornado was associated with the storm of interest at any time during its life. Though the Storm Events Database contains the most rigorously verified tornado dataset available, the absence of tornado reports does not guarantee that a particular storm did not produce a tornado, particularly a weak and/or short-lived tornado (e.g., Tanamachi et al. 2013). A comparison of warning statistics indicated that tornado and/or severe thunderstorm warnings were issued for 93.8% of nontornadic storms but only 81.3% of tornadic storms, indicating that the nontornadic storms were of sufficient intensity to warrant a warning. Tornado warnings were rarely issued for the nontornadic storms (12.5%).

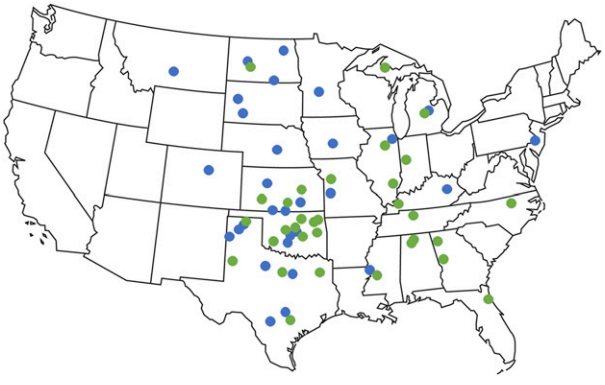

FIG. 1. Approximate locations of the 31 nontornadic storms (blue dots) and 32 pretornadic storms (green dots) included in the analysis.

Though tornado warnings were often issued for tornadic storms (78.1%), there was still a >20% rate of unwarned tornadic storms, motivating such work as reported here to investigate whether polarimetric radar signatures could increase confidence in a tornado warning decision.

Each radar scan included in the analysis window for each pretornadic and nontornadic storm was analyzed by computing values of several metrics, described below. Metrics were calculated using GIS software (for metrics requiring a size calculation), image processing software (for metrics requiring a mean value calculation), and cursor output within radar display software (for Z_{DR} column altitude). Excepting Z_{DR} column size and altitude, all metrics were calculated using 1-km CAPPIs of radar variables derived by inverse distance weighting-squared interpolation, reducing potential error due to metrics being calculated at differing altitudes through time or between storms. Metrics calculated include:

1) Areal extent of large hail (km^2; illustrated by Van Den Broeke 2016) was calculated as the area of the storm core over which $Z_{HH} > 55$ dBZ was collocated with Z_{DR} between -0.5 and $+1.0$ dB (e.g., Kumjian and Ryzhkov 2008a; Park et al. 2009). This metric could not be calculated for one pretornadic and eight nontornadic storms because there were not enough successive scans with base-scan hail area ≤1 km ARL. Additionally, in one pretornadic storm the storm-core Z_{HH} was <55 dBZ, though a localized Z_{DR} minimum with $-0.5 < Z_{DR} < 1$ dB collocated with the highest Z_{HH} values was strong evidence of hail so this case was retained.
2) Maximum storm-core Z_{HH} (dBZ) was the average of the 10 highest Z_{HH} bin values associated with the storm core, thought to represent precipitation intensity and hail likelihood. Note that Van Den Broeke (2017) used the single highest Z_{HH} value, which is more prone to noise. Pearson's correlation between results of the two methods was 0.995, with the single-pixel method yielding a value ~1.7 dBZ higher on average. An area-based metric may be optimal (e.g., the top 5% of bin values associated with storm area >35 dBZ) given beam spreading with distance and therefore poorer observation of localized maxima. For this dataset, however, maximum storm-core Z_{HH} did not appear to be affected by distance from the radar (Pearson's correlation = 0.068). This metric could not be calculated for 2 pretornadic and 7 nontornadic storms because there were not enough successive scans in which the storm core Z_{HH} at base-scan was ≤1 km ARL.
3) Z_{DR} arc size (km^2) was defined as the portion of the Z_{DR} arc (Kumjian and Ryzhkov 2008a) with values ≥3.5 dB (illustrated by Van Den Broeke 2016). This threshold well captured the core of the Z_{DR} arc and its temporal changes across this dataset of storms; sensitivity to the threshold choice is described below. This metric was not calculated for 3 pretornadic and 9 nontornadic storms because there were not enough successive scans with the Z_{DR} arc fully ≤1 km ARL or because data quality was poor in the storm inflow region.
4) Z_{DR} arc mean value (dB; Van Den Broeke 2016) was calculated as the mean value of all Z_{DR} arc bins with a value ≥3.5 dB. This contrasts with the method of Van Den Broeke (2016), who calculated this metric as the mean of all bins with a value ≥0 dB. This metric could not be calculated for 4 pretornadic and 9 nontornadic storms because there were not enough successive scans in which the Z_{DR} arc was fully ≤1 km ARL or because data quality was poor in the storm inflow region.
5) Z_{DR} arc width (km) was the width of the 2-dB arc measured perpendicular to the forward flank. Since Z_{DR} arc width often varies downstream from the mesocyclone region, an average value was calculated. This metric could not be calculated for 3 pretornadic and 9 nontornadic storms because there were not enough successive scans in which the Z_{DR} arc was fully ≤1 km ARL or because data quality was poor in the storm inflow region.
6) Z_{DR} column size (km^2), pictured by Van Den Broeke (2016), was calculated as the area of the 0.5-dB Z_{DR} column at an altitude ~1 km above the environmental 0°C level. The 0°C level was determined from archived RAP model output. An altitude ~1 km above this level was required since Z_{DR} columns are generally well-defined by that altitude. A Z_{DR} threshold of 0.5 dB was chosen since ice-phase scatterers at this altitude typically have $Z_{DR} <$ 0.5 dB. The elevation angle providing data nearest the required altitude was selected for analysis. Selected scans were typically ±300 m from the environmental 0°C level, with a maximum allowable value of ±500 m. Features identified as Z_{DR} columns were required to be vertically continuous with the high-Z_{DR} region below and collocated with the storm's high-Z_{HH} core or with a weak echo region. This metric could not be calculated for 2 pretornadic storms because data quality was poor in the storm updraft region.
7) Z_{DR} column depth (km) was calculated as the height at the top of the 1-dB Z_{DR} column minus altitude of the environmental 0°C level (Van Den Broeke 2016). The 1-dB threshold is consistent with the algorithm of Snyder et al. (2015). Column

identification again required vertical continuity and collocation with the storm's high-Z_{HH} core or with a weak echo region. Times were removed for which storms were too close to the radar for the Z_{DR} column to be fully sampled (e.g., the top of the column fell within the cone of silence). Since there are often large differences in beam centerline altitude between successive elevation angles, error in estimates of this metric is potentially large, especially at large range. This metric could not be calculated for two pretornadic storms because data quality was poor in the storm updraft region.

8) Mean appendage Z_{HH} was calculated using the method of French et al. (2015) to identify the echo appendage, and the mean Z_{HH} value within that area was calculated subject to a Z_{HH} threshold of 30 dBZ and ρ_{hv} threshold of 0.95 to exclude tornadic debris and dry hail. To be consistent with the appendages over which Z_{HH}–Z_{DR} plots were compared (metric 11 below), mean appendage Z_{HH} was only calculated if the appendage Z_{DR} was not influenced by nonmeteorological scatterers (e.g., tornadic debris) or other degrading features such as beam blockage. This led to the exclusion of 13 pretornadic and 13 nontornadic cases.
9) Mean appendage ρ_{hv} was calculated over the same area as defined for other echo appendage metrics, with a Z_{HH} threshold of 30 dBZ and a mean appendage ρ_{hv} threshold of $\geq$0.95 again applied. Given data quality issues with ρ_{hv}, this metric could not be computed for 13 pretornadic and 13 nontornadic storms (see Van Den Broeke 2016 for a list of reasons why cases were removed).
10) Mean appendage Z_{DR} (dB) was calculated using the same appendage area as for metrics 8 and 9. As with mean appendage ρ_{hv}, cases were excluded if tornadic debris or dry hail were indicated. In total, 13 pretornadic and 13 nontornadic cases were excluded.
11) Proportion of Z_{HH}–Z_{DR} points within the echo appendage falling above the C08 curve was calculated for the same appendage regions as in metrics 8–10. As in French et al. (2015), a ρ_{hv} lower threshold of 0.95 was used. As with mean appendage Z_{DR}, 13 pretornadic and 13 nontornadic storms were excluded when this metric was calculated.

It is clear from the number of storms excluded for some of the metrics, especially those related to echo appendage characteristics, that this should be seen as a preliminary study with a need for additional work utilizing a larger number of storms. In addition, some of the resulting n values are as low as 18 individual storms. A larger number of storms will increase the statistical robustness of such comparisons.

Once all values for a given metric for a single storm were calculated, a median value of that metric was calculated for that single storm. Mean metric values were also calculated for each storm using the population of all values from that storm. The mean values are not shown in this paper, but the interpretation of results was identical whether the mean or median values were used. Thus, the median was selected as a more outlier-resistant measure. Areal extent variables were normalized by storm size [defined as storm area with $Z_{HH} > 35$ dBZ, as by Van Den Broeke (2017)], though both normalized and nonnormalized measures were retained for the analysis. Also as in Van Den Broeke (2017), the coefficient of variation was used to quantify the variability of each radar metric through the analysis window for each storm. Given a set of values, the coefficient of variation is defined as the set's standard deviation normalized by the set's mean value, allowing comparison of the variability between storms with widely differing mean values of a particular metric. The coefficient of variation was only calculated for the 30 and 25 min prior to tornadogenesis, because for shorter analysis periods the standard deviation was often very high for strongly variable radar metrics and was not comparable with others, which were based on a larger sample size.

Z_{DR} calibration was achieved for all storms following the scatterer-based method of Picca and Ryzhkov (2012) and applied by Van Den Broeke (2017)—the resulting calibration factor was applied to all radar metrics that require Z_{DR}. For example, the 3.5-dB threshold used to define the Z_{DR} arc core was adjusted upward or downward for each individual storm to account for that storm's calibration factor. For the nontornadic storms, the mean calibration factor was −0.103 dB, comparable to the value of −0.07 dB for a sample largely overlapping the pretornadic storms in this study, reported by Van Den Broeke (2017). Among the nontornadic storms, the calibration factor exceeded 0.2 dB in 50% of events and 0.5 dB in 6% of events.

Wilcoxon–Mann–Whitney (WMW) statistics were utilized for the comparison of pretornadic and nontornadic storms, with a null hypothesis that radar metric median or coefficient of variation values from each set of storms could have come from the same distribution. This test was used to generate p values assuming that populations (e.g., of radar metric medians) may be non-Gaussian and that sample sizes may be small (e.g., Corder and Foreman 2014). By themselves p values are not authoritative evidence for or against a particular hypothesis, but they can increase confidence that a hypothesized physical mechanism is contributing (e.g., Wasserstein and Lazar 2016).

TABLE 3. Environmental variables with an ability to separate pretornadic from nontornadic storms in this sample (WMW p value ≤ 0.01).

Variable	Mean, pretornadic	Mean, nontornadic	WMW p value
Lifting condensation level (m)	453.6	1058.6	0.0015
Effective storm relative helicity ($m^2 s^{-2}$)	215.1	132.7	0.0097
Significant tornado parameter	2.31	0.65	0.0081
Lifting condensation level temperature (°C)	18.3	13.8	0.0008
0–1 km storm relative helicity ($m^2 s^{-2}$)	218.3	108.3	0.0014
0–3 km storm relative helicity ($m^2 s^{-2}$)	294.5	198.0	0.0063
0–1 km shear ($m s^{-1}$)	8.7	5.0	<0.0000
0–3 km shear ($m s^{-1}$)	15.9	12.3	0.0018

Environments of nontornadic supercells were characterized using the same variables as described by Van Den Broeke (2017) for the pretornadic storms (see Table 2 of that paper for a list of environmental variables included). In summary, the closest hourly Rapid Update Cycle (RUC) or Rapid Refresh (RAP) model initialization was selected relative to the center of the analysis period of each storm. Soundings were selected to be representative of the undisturbed far-field environment (e.g., as in Thompson et al. 2003, 2007). Error could have been introduced by the presence of undetected environmental heterogeneities (which were carefully screened for using satellite, surface, and radar data) and by the biases inherent to RUC and RAP (e.g., Benjamin et al. 2016). Storm-scale environmental variations, which may be critically important (e.g., Parker 2014), were also not able to be detected. Thus, soundings selected are generally representative of the synoptic-scale environment in which storms were embedded. Environments of tornadic and nontornadic storms were compared to get a sense for how well environmental characteristics distinguish these storm categories among this sample of storms and to ensure that the environments of these samples of storms are representative of 'typical' pretornadic and nontornadic environments.

3. Environments of supercells analyzed

This section describes differences between the environments of pretornadic and nontornadic supercell storms used in this study, to show that the environments of these storm samples are generally consistent with known differences between tornadic and nontornadic supercells. Accordingly, the radar signatures of these storms are thought to be a representative sample. Though a large set of environmental variables was examined [Table 2 of Van Den Broeke (2017)], only those with a WMW p value <0.01 are discussed here (see Table 3). The pretornadic and nontornadic storm datasets were generally distinguishable using environmental factors, as found in prior studies. Environmental differences such as those described here may influence storm structural and microphysical characteristics and therefore their radar signatures, so some of the radar differences noted in the following section may result from environmental differences, emphasizing the value of a future study examining radar signatures between storms in similar environments.

Tornadic environments are often distinguished by low mixed-layer lifting condensation level (MLLCL) height (e.g., Thompson et al. 2003), which was also the case for this sample of storms (Fig. 2a, Table 3)—mean MLLCL height was more than twice as high among the nontornadic storms. Pretornadic storms also tended to be associated with warmer environments, evidenced by their warmer MLLCL temperatures (Table 3; Fig. 2b). These results did not appear to be due to storms occurring at different times of year—median Julian day was similar [139.5 for pretornadic storms (mid-May) and 150.0 for nontornadic storms (late May)].

As expected given prior studies (e.g., Thompson et al. 2003; Parker 2014; Tochimoto and Niino 2016; Taszarek et al. 2017), wind variables in the lowest 3 km strongly separated pretornadic and nontornadic supercells. Vertical wind shear was much stronger in the 0–1 km (Fig. 2c) and 0–3 km (Table 3) layers among pretornadic storms. SRH estimated using Bunkers storm motion (Bunkers et al. 2000) was also significantly higher in the 0–1 km (Fig. 2d) and 0–3 km (Table 3) layers among pretornadic storms. For both wind shear and SRH variables, the near-surface layer (0–3 km) had the best ability to separate pretornadic from nontornadic storms. When SRH in an effective inflow layer was examined (e.g., Thompson et al. 2007), the same strong distinguishing ability existed (Fig. 2e, Table 3). The significant tornado parameter (STP; Rasmussen and Blanchard 1998; Parker 2014), a composite parameter incorporating wind and instability information, was 3.5 times larger among pretornadic storms (Table 3).

In summary, environmental variables well-distinguished these samples of pretornadic and nontornadic storms, and the variables allowing separation are as expected from prior studies. This indicates that the sample's radar signatures are also likely representative.

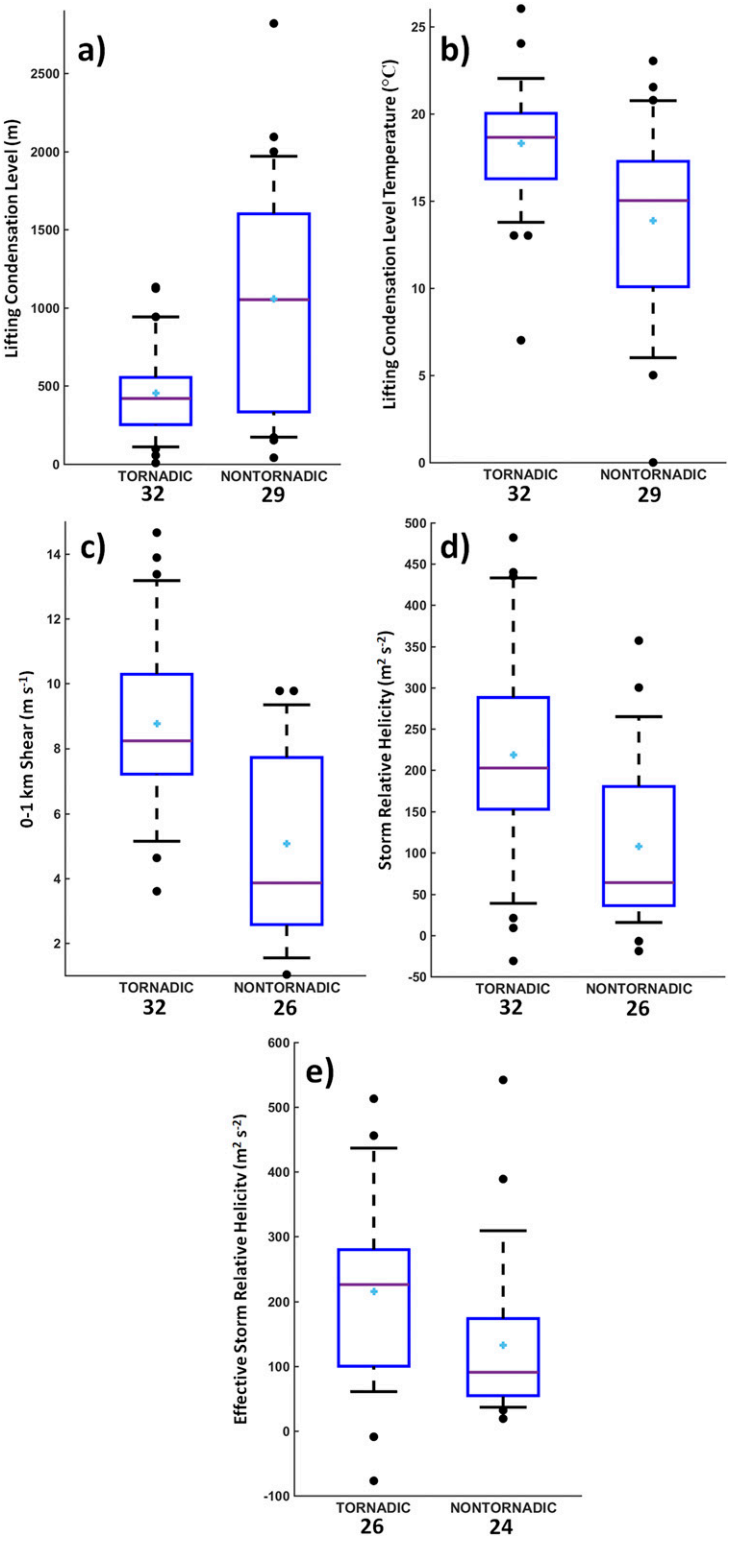

FIG. 2. Comparison of environmental variables between the pretornadic and nontornadic storms: (a) MLLCL height (m), (b) MLLCL temperature (°C), (c) 0–1 km shear (m s^{-1}), (d) 0–1 km storm relative helicity ($m^2 s^{-2}$), and (e) effective-layer storm relative helicity ($m^2 s^{-2}$). The bottom of each blue box is the first quartile, and the top of each blue box is the third quartile. The purple bar indicates the median value, and the light blue "+" indicates the mean value. Outlying horizontal bars are at the 9th and 91st percentiles, with outliers indicated as filled circles. Numbers below the *x* axis indicate the number of values used to construct each boxplot.

TABLE 4. Left two columns of values indicate the median (MED) values of polarimetric radar metrics compared between samples of nontornadic (NT) and pretornadic (PT) supercell storms in the 30 min prior to initial tornadogenesis. Following columns indicate the WMW p values for a comparison of the distributions of medians when pretornadogenesis analysis periods of 30, 25, 20, and 15 min are used for the PT storms. "N" next to the variable name indicates normalization by storm size. WMW p values < 0.01 are boldface and italic and WMW p values $0.05 > p > 0.01$ are boldface only. Units are indicated in brackets next to the name of each variable; "[ ]" indicates a unitless quantity.

	PT 30 min period		p value lead time for PT supercells:			
Radar metric	MED (PT)	MED (NT)	30 min	25 min	20 min	15 min
Storm size [km^2]	633	668	0.994	0.908	0.795	0.724
Hail areal extent [km^2]	23.1	50.3	**0.020**	**0.016**	**0.022**	**0.014**
Hail areal extent (N) [ ]	0.04	0.08	**0.018**	**0.020**	**0.017**	**0.014**
Z_{HH} max storm core value [dBZ]	63.8	66.2	**0.033**	**0.038**	**0.023**	**0.038**
Z_{DR} arc size [km^2]	63.1	42.5	0.162	0.186	0.146	0.104
Z_{DR} arc size (N) [ ]	0.12	0.08	0.082	0.096	0.075	0.064
Z_{DR} arc width [km]	7.01	6.15	0.151	0.174	0.092	0.206
Z_{DR} arc mean value [dB]	4.55	4.52	0.977	0.977	0.837	0.500
Z_{DR} column size aloft [km^2]	71.7	41.0	***0.005***	***0.003***	***0.005***	***0.003***
Z_{DR} column size aloft (N) [ ]	0.11	0.07	***0.002***	***0.001***	***0.001***	***0.001***
Z_{DR} column depth [km]	2.76	2.48	0.264	0.166	0.171	0.134
Mean appendage Z_{HH} [dBZ]	35.8	38.1	0.098	0.161	0.181	0.204
Mean appendage ρ_{hv} [ ]	0.965	0.970	0.186	0.176	0.113	0.146
Mean appendage Z_{DR} [dB]	2.31	1.77	**0.013**	**0.010**	**0.042**	0.083
% appendage above C08 curve	67.4	59.4	**0.032**	**0.031**	0.096	0.089

4. Differences between pretornadic and nontornadic supercell storms

a. *Storm size, hail areal extent, and storm-core Z_{HH} values*

It was hypothesized that pretornadic supercells would be characterized by a more variable hail signature and therefore a smaller mean hail areal extent and lower storm-core Z_{HH} values. Hail extent was normalized by storm size (km^2, defined as area of $Z_{HH} > 35$ dBZ). Among this sample of storms, storm size was ~5.6% larger for nontornadic storms, but statistically similar (Table 4; Fig. 3a). Variability of storm size was also statistically similar between pretornadic and nontornadic storms (Table 5).

Storm-core maximum Z_{HH}, calculated as the mean of the 10 highest-valued bins, can be an indicator of hail size and/or the presence of melting hail (e.g., Ryzhkov et al. 2010). Given the potential importance of large and melting hail to low-level storm thermodynamics and potential differences in hail characteristics of tornadic and nontornadic storms observed prior (e.g., Kumjian and Ryzhkov 2008a, 2009), it is hypothesized here that this variable may be indicative of whether a storm is pretornadic or will remain nontornadic. Polarimetric measurements such as hail differential reflectivity (Depue et al. 2007) may also be insightful but were not investigated here. Over all 440 pretornadic and nontornadic analysis periods, the 10th percentile was 58.4 dBZ with a mean value of 65.3 dBZ—while $Z_{HH} < 55$ dBZ can indicate hail, this is usually assumed to indicate relatively small wet hail (e.g., Straka et al. 2000). Median storm-core maximum Z_{HH} was 2.4 dBZ higher in the nontornadic storms with a pretornado lead time of 30 min (Table 4; Fig. 3b), a statistically significant result (p = 0.023–0.038 at lead times of 15–30 min; Table 4). Figure 4 shows a representative distribution of Z_{HH} for a pretornadic (Fig. 4a) and a nontornadic (Fig. 4b) storm. Variability of this metric did not distinguish pretornadic and nontornadic storms (Table 5). The degree to which this variable provides similar information to hail areal extent was briefly investigated. Though there is a positive relationship between storm-core maximum Z_{HH} and hail areal extent, Pearson's correlation between the two variables indicates that they may contain separate, useful information (p = 0.596 [pretornadic] and p = 0.453 [nontornadic]).

The size of the inferred polarimetric hail signature was compared between pretornadic and nontornadic supercells; for consistency with past studies, both raw values and values normalized by storm size were compared (Table 4; Figs. 3c,d). Both had about the same ability to distinguish whether a storm was pretornadic or nontornadic (p = 0.014–0.020 for normalized hail signature size and p = 0.014–0.022 for raw hail signature size for 15–30 min prior to tornadogenesis). Hail extent tended to be most diagnostic in the 15–20 min prior to initial tornadogenesis (Table 4). Though variability of hail extent was larger in pretornadic storms, this was not statistically significant (Table 5). These findings support the hypothesis that nontornadic supercells contain hail

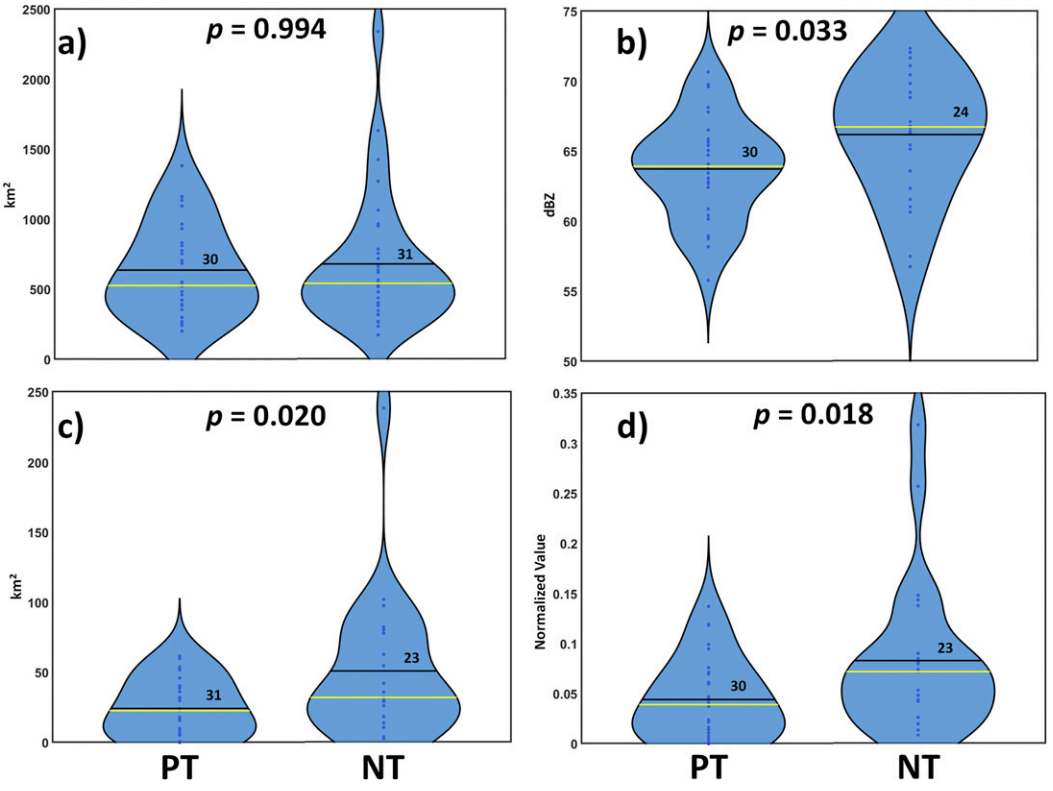

FIG. 3. Violin plots showing the distribution of (a) storm size (km^2), (b) maximum storm-core Z_{HH} values (dBZ), (c) raw hail areal extent (km^2), and (d) normalized hail areal extent, all at an altitude of 1 km ARL. Left column of each pair is for pretornadic storms (PT), and right column is for nontornadic storms (NT). PT values are valid for the 30-min period prior to initial tornadogenesis. Number of storms contributing to each violin indicated within each violin, and raw values indicated as points. In each violin, the black line is the mean and the yellow line is the median. The p value for each comparison is included in each panel.

over a larger relative area but do not statistically support that hailfall is less variable in nontornadic storms. Figure 4 shows a typical example of hailfall in pretornadic (Figs. 4a,c) and nontornadic (Figs. 4b,d) supercells—the nontornadic storm has a large region with hail (indicated by the white outline in Figs. 4b and 4d), while the pretornadic storm has a much smaller hail region (Figs. 4a,c). Hail areal extent never exceeded 112 km^2 (and rarely 80 km^2) among the pretornadic storms (Fig. 3c), and hail extent this large among nontornadic storms was often accompanied by a storm-core Z_{HH} maximum value >62 dBZ (not shown).

b. Z_{DR} arc characteristics

Z_{DR} arcs are indicative of hydrometeor size sorting in storm-relative inflow winds along the forward flank. In this paper they are hypothesized to be less variable in width and mean value in pretornadic supercells than in nontornadic supercells due to less consistent hailfall disruptions. Z_{DR} within the arcs of pretornadic storms is also hypothesized to be higher given a possible smaller contribution from melting hail. In prior studies Z_{DR} arc characteristics have been related to tornado life cycles (e.g., Palmer et al. 2011; Crowe et al. 2012), and some preliminary differences have been noted between samples of tornadic and nontornadic storms (Van Den Broeke 2016). The magnitude of Z_{DR} values within the arc has also been related to the magnitude of low-level shear and SRH (e.g., Kumjian and Ryzhkov 2009; Dawson et al. 2015). Among this sample of storms, mean Z_{DR} value within the arc was weakly correlated to 0–1 and 0–3 km shear (r = 0.169 and r = 0.267, respectively) and weakly correlated to 0–1 km SRH and 0–3 km SRH (r = 0.216 and r = 0.268, respectively), generally in support of these prior findings.

To test the appropriateness of the 3.5-dB Z_{DR} threshold used to define the Z_{DR} arc, varying Z_{DR} thresholds were tested on a random sample of 7 pretornadic and 8 nontornadic storms from this dataset. When thresholds of 1.5, 2, 2.5, 3, 3.5, and 4 dB were selected, the typical pattern was for low thresholds to produce very

TABLE 5. As in Table 4, but for coefficient of variation (CoV) in and 30 and 25 min prior to tornadogenesis.

Radar metric	PT 30 min period		p value lead time for PT supercells:	
	CoV (PT)	CoV (NT)	30 min	25 min
Storm size [km^2]	0.12	0.13	0.276	0.155
Hail areal extent [km^2]	0.66	0.41	0.094	0.106
Hail areal extent (N) [ ]	0.67	0.44	0.176	0.182
Z_{HH} max storm core value [dBZ]	0.02	0.02	0.389	0.196
Z_{DR} arc size [km^2]	0.42	0.41	0.977	0.802
Z_{DR} arc size (N) [ ]	0.43	0.53	0.213	0.175
Z_{DR} arc width [km]	0.19	0.19	0.783	0.725
Z_{DR} arc mean value [dB]	0.06	0.08	**0.029**	**0.034**
Z_{DR} column size aloft [km^2]	0.28	0.47	***0.002***	***0.003***
Z_{DR} column size aloft (N) [ ]	0.32	0.50	**0.029**	**0.035**
Z_{DR} column depth [km]	0.19	0.27	**0.041**	**0.041**
Mean appendage Z_{HH} [dBZ]	0.09	0.08	0.323	0.482
Mean appendage ρ_{hv} [ ]	0.016	0.007	0.054	**0.039**
Mean appendage Z_{DR} [dB]	0.18	0.17	0.727	0.826
% appendage above C08 curve	0.10	0.11	0.111	0.459

large areal extents that include much of the supercell area. Some intermediate thresholds produce roughly parallel areas, while the highest threshold (4 dB) occasionally produced no area. Pearson's correlation was calculated between arc area from successive Z_{DR} thresholds, and comparisons yielding correlation $\geq$0.70 were interpreted as indicating that a similar feature (the true Z_{DR} arc) was being identified. The minimum and maximum threshold values associated with a correlation of at least 0.7 were recorded for each storm. Across all storms, the average minimum threshold value that well characterized the Z_{DR} arc was 2.03 dB, and the average maximum threshold value was 3.47 dB. These closely correspond to the prior-chosen subjective values (e.g., Van Den Broeke 2017) of 2 dB for Z_{DR} arc width and 3.5 dB for Z_{DR} arc area. Thus, these two threshold values appear to reasonably well characterize the Z_{DR} arcs of the storms examined.

Variability of Z_{DR} arc metrics was generally statistically similar between pretornadic and nontornadic storms, except for Z_{DR} arc mean bin value which was more variable in nontornadic storms (p = 0.029–0.034 at lead times of 25–30 min; Table 5). Not all Z_{DR} arc metrics were more variable in nontornadic storms (Table 5), lending little support to the hypothesis that the arc is more consistently disrupted by hail in nontornadic storms. The median value of Z_{DR} within the Z_{DR} arc was effectively the same between pretornadic and nontornadic storms (Table 4; Fig. 5), not supporting the hypothesis that Z_{DR} values within the arc should be larger in pretornadic storms. These findings generally indicate that pretornadic and nontornadic storms may not be separable using basic Z_{DR} arc characteristics. Though not statistically significant, Z_{DR} arcs were often larger in pretornadic storms (by an average of ~48%; Table 4; Figs. 5a,b), an observation that may warrant further investigation.

c. Z_{DR} column characteristics

Z_{DR} columns are representative of the updraft region in deep convective storms including supercells (e.g., Kumjian and Ryzhkov 2008a; Kumjian et al. 2010, 2014; Houser et al. 2015; Van Den Broeke 2016; and others), and updraft strength changes may be inferred polarimetrically by utilizing characteristics of this signature. Given prior observations (e.g., Van Den Broeke 2016, 2017), it is hypothesized that updrafts may be larger, deeper, and steadier in pretornadic supercells. In contrast to Z_{DR} arc characteristics, Z_{DR} columns did distinguish pretornadic and nontornadic supercells in this sample of storms.

The size of the 0.5-dB Z_{DR} column (corrected for calibration offset) approximately 1 km above the ambient 0°C level was ~55% larger in pretornadic storms (using data from the 30 min prior to tornadogenesis) when the value was normalized by storm size (p = 0.001–0.002 at lead times of 15–30 min; Table 4; Fig. 6b). Figure 7 shows an example of typical Z_{DR} column appearance in pretornadic (Figs. 7a,c) and nontornadic (Figs. 7b,d) supercells (white outline indicates Z_{DR} column location). At 1 km above the ambient 0°C level, Z_{DR} columns of pretornadic storms were more likely to be nearly the size of the central high-Z_{HH} region (as in Figs. 7a,c), while in nontornadic storms the Z_{DR} column was often more isolated to small portions of the high-Z_{HH} region (as in Figs. 7b,d). This observation may be related to possible masking of the column by the large quantity of hail in many nontornadic storms. Supporting this possibility, a correlation value of −0.356 was found

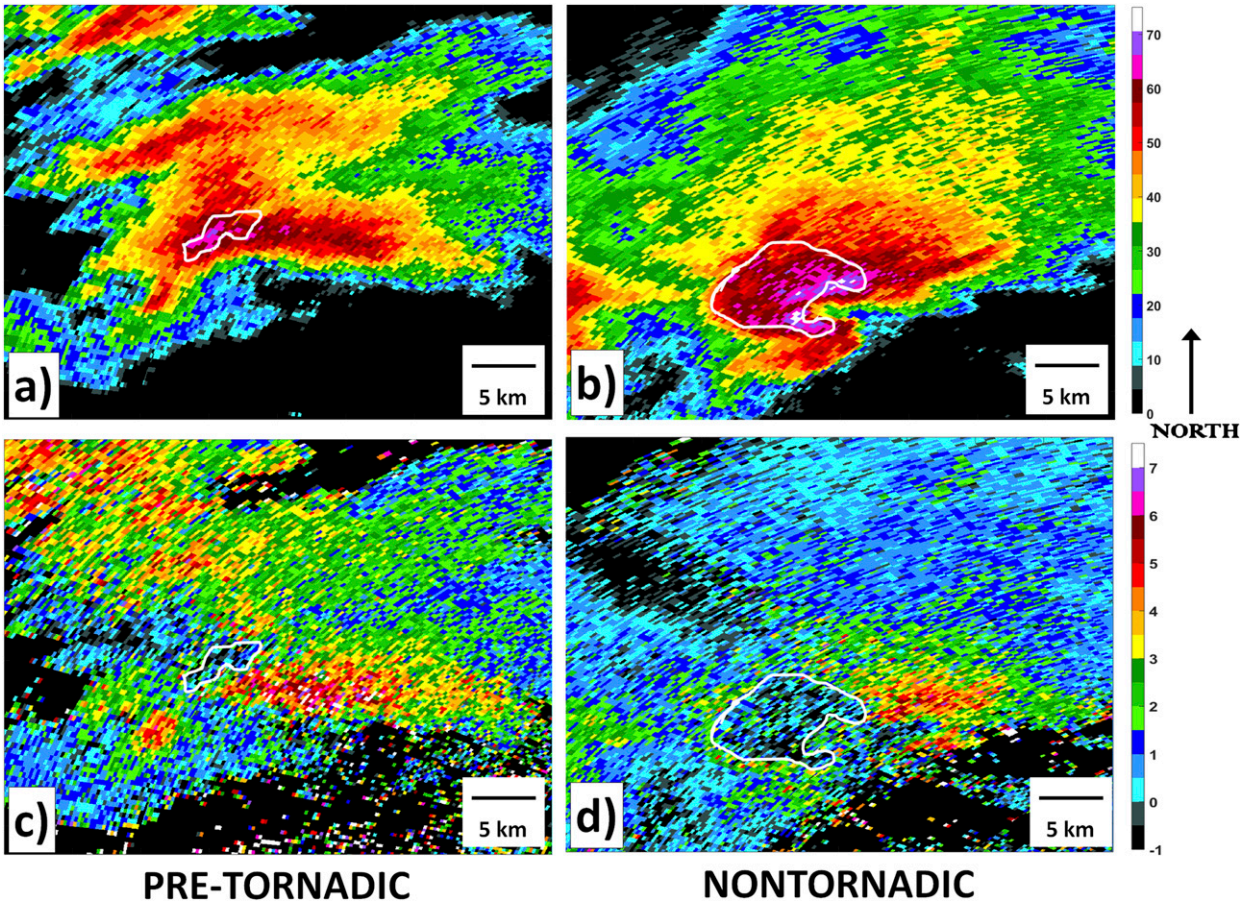

FIG. 4. 1-km comparison of pretornadic and nontornadic supercell storms. (a),(c) Tulsa, Oklahoma, radar (KINX; at 2039 UTC 20 May 2013), and range to storm core is approximately 63 km. (b),(d) Bismarck, North Dakota, radar (KBIS; at 0553 UTC 4 Sep 2014); range to storm core is approximately 66 km. White outlines represent areas of polarimetrically inferred hailfall; Z_{DR} calibration factors of −0.05 dB (KINX) and −0.62 dB (KBIS) have been applied to the data shown here.

between storm-mean normalized hail extent and normalized Z_{DR} column area using all storms in this dataset (larger hail extent generally corresponded to a smaller Z_{DR} column). Median pretornadic Z_{DR} column depth was also ~0.27 km greater over the 30 min prior to tornadogenesis (Table 4; Fig. 6c), though this difference was not significant. Measures of Z_{DR} column size and depth variability statistically separated pretornadic and nontornadic storms and were larger among nontornadic storms (Table 5). Z_{DR} column size normalized by storm area was ~58% more variable and Z_{DR} column depth ~42% more variable among nontornadic storms when compared with the 30 min prior to tornadogenesis. These differences did not appear to be a function of environmental CAPE, which was statistically similar between the two populations of storms ($p = 0.39$). In aggregate, these findings support the hypothesis that updrafts are steadier, deeper, and spatially larger in pretornadic storms.

d. *Echo appendage characteristics*

In this paper it is hypothesized that echo appendages of pretornadic storms contain less melting hail, which may be detectable as smaller mean Z_{HH} and Z_{DR}, larger mean ρ_{hv}, and fewer bins falling above the C08 curve. Among this sample of storms, median Z_{HH} was ~2.3 dBZ larger in the nontornadic appendages compared to the 30 min prior to tornadogenesis (Fig. 8a; Table 4), which often appeared to be related to increased prevalence of small hail in appendages of nontornadic storms, similar to a hypothesis of Kumjian and Ryzhkov (2008b). This pattern was not, however, consistent across the set of nontornadic storms. Note that the ρ_{hv} threshold of 0.95 used to filter appendage bins for the purpose of averaging would generally remove dry hail, but might not exclude all bins with wet/melting hail. Median appendage ρ_{hv} was similar between pretornadic and nontornadic storms (Fig. 8b; Table 4), not as hypothesized. Median Z_{DR} was 0.54 dB higher in pretornadic storms (Fig. 8c), indicating

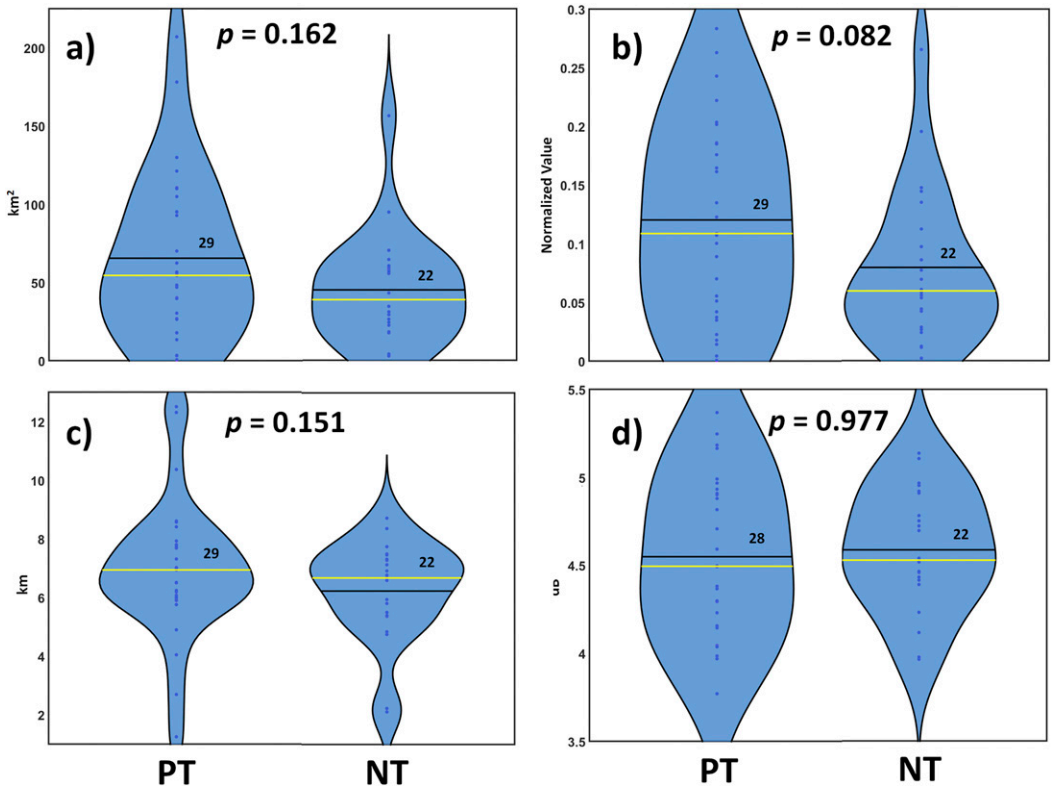

FIG. 5. As in Fig. 3, but for (a) raw Z_{DR} arc size (km^2), (b) normalized Z_{DR} arc size, (c) Z_{DR} arc width (km), and (d) mean Z_{DR} value within the Z_{DR} arc (dB).

larger drops. This result was significant (Table 4; p = 0.010–0.042 at 20–30 min). Future work is needed, as this finding contrasts with French et al. (2015) and Kumjian and Ryzhkov (2008b), who found evidence for smaller drops in the appendages of tornadic storms. The difference between pretornadic and nontornadic storms was not significant for a lead time of 15 min (Table 4). As expected given the larger Z_{DR} values in pretornadic storms, the percentage of appendage Z_{HH}–Z_{DR} points above the C08 curve (indicating a drop distribution with large median diameter) in these storms was also ~14% larger in the 30 min prior to tornadogenesis (Fig. 8d; Table 4; p = 0.031–0.032 at leads times of 25–30 min), not supporting the hypothesis of larger mean drops in nontornadic storms. A relatively large percentage of bins above the C08 curve in both supercell categories indicate appendages dominated by relatively large drops, consistent with the findings of Kumjian and Ryzhkov (2008b).

In aggregate and for this sample of storms, these results provide evidence against the hypothesis that nontornadic appendages contain larger median drops. Given these and prior findings (e.g., French et al. 2015; Kumjian and Ryzhkov 2008b), additional research seems warranted to construct a climatology of appendage characteristics in supercell storms. Additional understanding of microphysics in this storm region (e.g., Kumjian 2011; Kumjian et al. 2015) is also needed.

5. Summary and discussion

Using a population of 19–30 pretornadic and 18–31 nontornadic supercells, several radar-derived metrics (Table 4) and their variability (Table 5) appear to separate supercells that are pretornadic from those that remain nontornadic. Some radar metrics did not show significant differences between pretornadic and nontornadic storms. It is important to note that such metrics should not be discarded from future supercell tornadogenesis studies since this study did not examine trends leading up to tornadogenesis. Even though temporal changes are somewhat conveyed by the analysis of different pretornadogenesis temporal windows in this study, a more detailed examination of trends would be needed. For instance, there may be value in examining whether the magnitude of the metrics is increasing or decreasing, how large these changes are through time, and if these changes are accelerating. Such a study could also be insightful if combined with a comparison of "pretornadogenesis failure" periods in nontornadic supercell storms. The relatively small number of storms

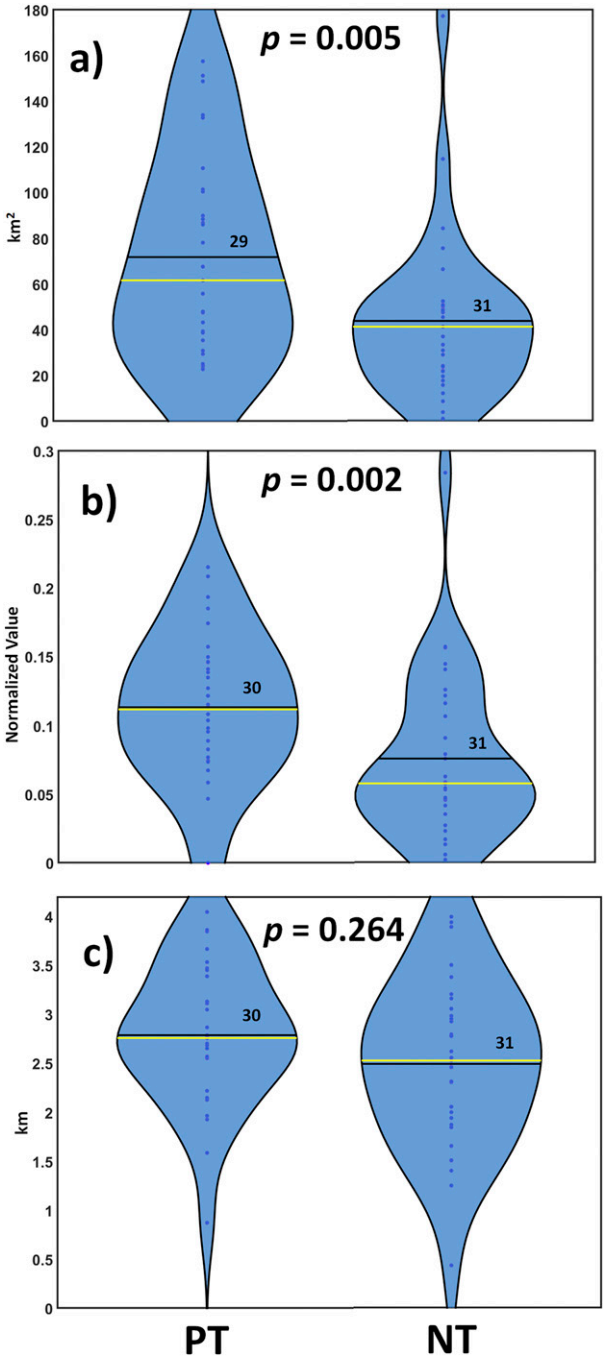

FIG. 6. As in Fig. 3, but for (a) Z_{DR} column size at 1 km above the ambient 0°C level (km^2), (b) normalized Z_{DR} column size, and (c) Z_{DR} column depth (km).

included for some of the metrics, especially those characterizing the echo appendage, also points to the need for future work, which examines much larger populations of storms in a climatological sense.

As hypothesized, pretornadic storms appear to have a smaller area of polarimetrically inferred hailfall, lower storm-core Z_{HH} values, and Z_{DR} columns that are larger, deeper, and steadier. Z_{DR} arc characteristics did not distinguish pretornadic and nontornadic storms, contrary to hypotheses. Variability of radar characteristics was generally slightly larger for pretornadic storms, though pretornadic storms exhibited less variability of Z_{DR} column size and depth. Updrafts in aggregate appeared to be larger, deeper, and steadier among the pretornadic storms—this was the case even though measures of instability (e.g., CAPE) were statistically similar between the pretornadic and nontornadic storms, though measures of wind shear were larger in pretornadic storm environments (Table 3). This suggests that more updraft ascent is dynamically driven among the pretornadic storms in this sample. Nontornadic storms were characterized by smaller/shallower Z_{DR} columns, larger hail areal extent, and larger storm-core Z_{HH} values—it is possible that the large hail content in nontornadic storms partially obscures their Z_{DR} columns. The difference in hail extent between pretornadic and nontornadic storms may be partially a function of the lower mean environmental 0°C level among the nontornadic storms, allowing more hail mass to survive to lower altitude. Pearson's correlation between normalized hail areal extent and environmental 0°C altitude for this dataset was −0.43 (r^2 = 0.185).

Z_{DR} arc characteristics did not well-distinguish pretornadic and nontornadic storms in this sample. Arcs were larger among pretornadic storms, which while not statistically significant may warrant additional investigation using a much larger sample of storms. Orientation of the Z_{DR} arc, while not investigated in this study, could be a beneficial focus of future research given the promising findings of prior studies (e.g., Palmer et al. 2011), as could separation of the Z_{DR}–K_{DP} maxima (e.g., Crowe et al. 2012; Loeffler and Kumjian 2018).

After additional research, several preliminary results presented in this paper may eventually be operationally useful to identify pretornadic storms, though application may be challenging because of radar data quality issues (e.g., Z_{HH} and Z_{DR} calibration). Some of the results noted here may eventually lead to guidance suggesting which storm(s) to focus on for future tornadic potential, given situations with numerous storms in the domain of a single radar. Less value may be realized when a single supercell is present, since in that situation it is not possible to compare metric values between storms. Such methods may also lead more to retrospective results than to prognostic value (as described by Kumjian and Ryzhkov 2008a). Future work examining tornadic and nontornadic supercells in close proximity, which may lead to clearer operational guidance, is warranted. The most promising

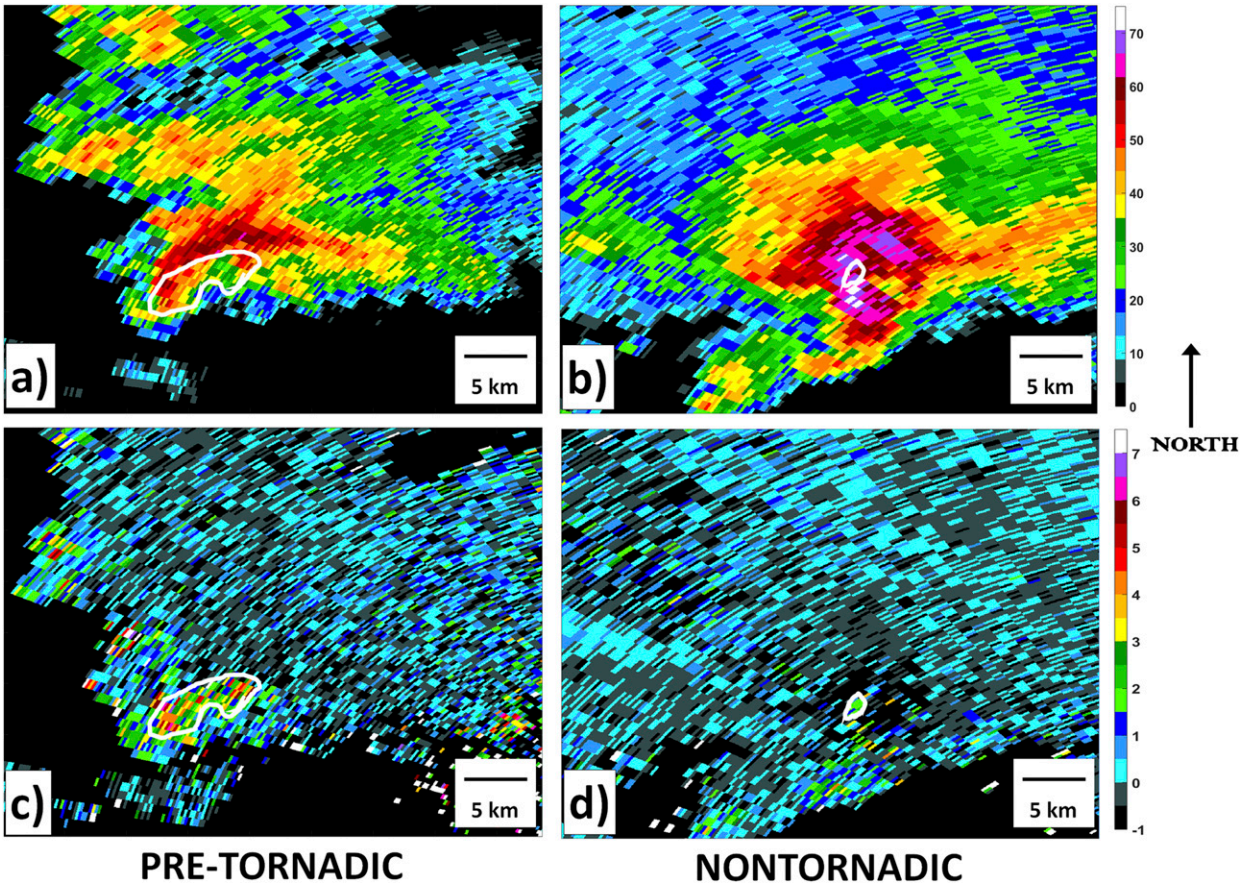

FIG. 7. Comparison of pretornadic and nontornadic supercell storms at an elevation ~1 km above the ambient 0°C level. (a),(c) Tulsa, Oklahoma, radar (KINX; at 2039 UTC 20 May 2013); elevation angle is 4.00°, and range to storm core is approximately 62 km (altitude of beam center ~4.55 km). (b),(d) are from the Bismarck, North Dakota, radar (KBIS; at 0553 UTC 4 Sep 2014); elevation angle is 5.10°, and range to storm core is approximately 53 km (altitude of beam center ~4.91 km). White outlines represent Z_{DR} columns. Z_{DR} calibration factors of +0.404 dB (KINX) and −0.62 dB (KBIS) have been applied to the data shown here.

topics for additional research suggested by the results in this paper include:

1) Smaller hail areal extent in pretornadic storms. It will be necessary to test whether this finding remains valid when tornadic and nontornadic storms are concurrently present. Such methods need to be carefully designed to ensure that natural variability is not having too large of an impact—e.g., by basing the radar time series on an analysis period of sufficient length, optimally over at least 20 min.
2) Higher storm-core maximum Z_{HH} in nontornadic storms. This could be particularly valuable in the domain of a single radar where calibration does not affect the results. As with hail extent, this result needs to be tested in situations when tornadic and nontornadic storms are present. Future work should consider using a percentile approach to define which bins are averaged, and should examine hail distributions within the appendages of pretornadic and nontornadic storms.
3) Substantially larger and steadier Z_{DR} columns among pretornadic storms. Though increased depth in pretornadic storms was not statistically significant, it may be worthy of additional investigation alongside other Z_{DR} column metrics.

Diagnosing whether a storm is more likely to become tornadic or remain nontornadic using the metrics described herein relies on careful assessment of data quality and storm behavior. For many of the metrics it is critical to determine a Z_{DR} calibration offset that is applied across the data, though insight is also possible if proximate storms can be compared (e.g., a similar calibration offset applies to all storms). Other data quality issues, such as three-body scatter downradial of hail, also need to be filtered out to avoid erroneous values in time series of some of the radar metrics. Finally, temporal

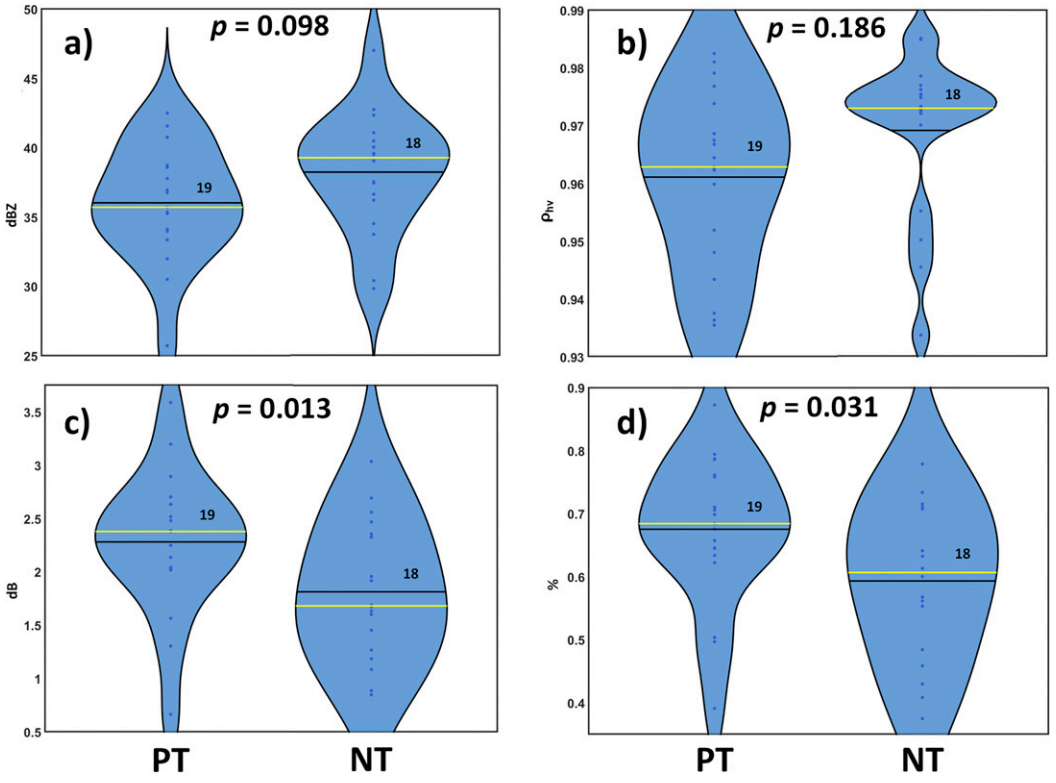

FIG. 8. As in Fig. 3, but for (a) mean appendage Z_{HH} (dBZ), (b) mean appendage ρ_{hv}, (c) mean appendage Z_{DR} (dB), and (d) percentage of points falling above the C08 curve (e.g., 0.5 = 50%).

variability of many of the radar metrics is large enough that median values should be determined over a minimum of ~20 min. Thus, while data from one or a few scans may be used to indicate potential that a storm is pretornadic, confidence in this diagnosis increases with the length of time over which a storm is analyzed. The results here indicate that hail variables may be useful in the 15–20 min prior to tornadogenesis, while Z_{DR} column and echo appendage characteristics may be most useful ~25 min prior to tornadogenesis. With additional work focused on volumes containing both tornadic and nontornadic storms, the results presented here may form a basis for additional operational guidance regarding the use of polarimetric radar metrics to assess the tornadic potential of particular supercell storms.

Acknowledgments. The author was supported by NSF Grant IIA-1539070, NOAA Grant NA18OAR4590307, and an academic appointment at the University of Nebraska–Lincoln. Nick Humrich and Matt Wilson are acknowledged for code contributions. The author acknowledges the reviews of three anonymous peer reviewers who substantially improved the focus and quality of early drafts.

REFERENCES

Benjamin, S. G., and Coauthors, 2016: A North American hourly assimilation and model forecast cycle: The Rapid Refresh. *Mon. Wea. Rev.*, **144**, 1669–1694, https://doi.org/10.1175/MWR-D-15-0242.1.

Bluestein, H. B., and J. C. Snyder, 2015: An observational study of the effects of dry air produced in dissipating convective storms on the predictability of severe weather. *Wea. Forecasting*, **30**, 79–114, https://doi.org/10.1175/WAF-D-14-00065.1.

Brooks, H. E., C. A. Doswell III, and J. Cooper, 1994: On the environments of tornadic and nontornadic mesocyclones. *Wea. Forecasting*, **9**, 606–618, https://doi.org/10.1175/1520-0434(1994)009<0606:OTEOTA>2.0.CO;2.

Brotzge, J., and W. Donner, 2013: The tornado warning process: A review of current research, challenges, and opportunities. *Bull. Amer. Meteor. Soc.*, **94**, 1715–1733, https://doi.org/10.1175/BAMS-D-12-00147.1.

Bunkers, M. J., B. A. Klimowski, J. W. Zeitler, R. L. Thompson, and M. L. Weisman, 2000: Predicting supercell motion using a new hodograph technique. *Wea. Forecasting*, **15**, 61–79, https://doi.org/10.1175/1520-0434(2000)015<0061:PSMUAN>2.0.CO;2.

Cao, Q., G. Zhang, E. Brandes, T. Schuur, A. Ryzhkov, and K. Ikeda, 2008: Analysis of video disdrometer and polarimetric radar data to characterize rain microphysics in Oklahoma. *J. Appl. Meteor. Climatol.*, **47**, 2238–2255, https://doi.org/10.1175/2008JAMC1732.1.

Coffer, B. E., and M. D. Parker, 2017: Simulated supercell in nontornadic and tornadic VORTEX2 environments. *Mon.*

Wea. Rev., **145**, 149–180, https://doi.org/10.1175/MWR-D-16-0226.1.

——, and P. M. Markowski, 2018: Comments on "The regulation of tornado intensity by updraft width." *J. Atmos. Sci.*, **75**, 4049–4056, https://doi.org/10.1175/JAS-D-18-0170.1.

Corder, G. W., and D. I. Foreman, 2014: *Nonparametric Statistics: A Step-by-Step Approach*. 2nd ed. Wiley, 288 pp.

Crowe, C. C., C. J. Schultz, M. Kumjian, L. D. Carey, and W. A. Petersen, 2012: Use of dual-polarization signatures in diagnosing tornadic potential. *Electron. J. Oper. Meteor.*, **13**, 57–78.

Davies, J. M., 2004: Estimations of CIN and LFC associated with tornadic and nontornadic supercells. *Wea. Forecasting*, **19**, 714–726, https://doi.org/10.1175/1520-0434(2004)019<0714:EOCALA>2.0.CO;2.

Dawson, D. T., E. R. Mansell, Y. Jung, L. J. Wicker, M. R. Kumjian, and M. Xue, 2014: Low-level Z_{DR} signatures in supercell forward flanks: The role of size sorting and melting of hail. *J. Atmos. Sci.*, **71**, 276–299, https://doi.org/10.1175/JAS-D-13-0118.1.

——, ——, and M. R. Kumjian, 2015: Does wind shear cause hydrometeor size sorting? *J. Atmos. Sci.*, **72**, 340–348, https://doi.org/10.1175/JAS-D-14-0084.1.

Depue, T. K., P. C. Kennedy, and S. A. Rutledge, 2007: Performance of the hail differential reflectivity (H_{DR}) polarimetric radar hail indicator. *J. Appl. Meteor. Climatol.*, **46**, 1290–1301, https://doi.org/10.1175/JAM2529.1.

Esterheld, J. M., and D. J. Giuliano, 2008: Discriminating between tornadic and non-tornadic supercells: A new hodograph technique. *Electron. J. Severe Storms Meteor.*, **3** (2), http://www.ejssm.org/ojs/index.php/ejssm/article/viewArticle/33.

Forbes, G. S., 1981: On the reliability of hook echoes as tornado indicators. *Mon. Wea. Rev.*, **109**, 1457–1466, https://doi.org/10.1175/1520-0493(1981)109<1457:OTROHE>2.0.CO;2.

French, M. M., D. W. Burgess, E. R. Mansell, and L. J. Wicker, 2015: Bulk hook echo raindrop sizes retrieved using mobile, polarimetric Doppler radar observations. *J. Appl. Meteor. Climatol.*, **54**, 423–450, https://doi.org/10.1175/JAMC-D-14-0171.1.

Houser, J. L., H. B. Bluestein, and J. C. Snyder, 2015: Rapid-scan, polarimetric, Doppler radar observations of tornadogenesis and tornado dissipation in a tornadic supercell: The "El Reno, Oklahoma" storm of 24 May 2011. *Mon. Wea. Rev.*, **143**, 2685–2710, https://doi.org/10.1175/MWR-D-14-00253.1.

——, ——, and ——, 2016: A finescale radar examination of the tornadic debris signature and weak-echo reflectivity band associated with a large, violent tornado. *Mon. Wea. Rev.*, **144**, 4101–4130, https://doi.org/10.1175/MWR-D-15-0408.1.

Klees, A. M., Y. Richardson, P. Markowski, C. Weiss, J. Wurman, and K. Kosiba, 2016: Comparison of the tornadic and nontornadic supercells intercepted by VORTEX2 on 10 June 2010. *Mon. Wea. Rev.*, **144**, 3201–3231, https://doi.org/10.1175/MWR-D-15-0345.1.

Kumjian, M. R., 2011: Precipitation properties of supercell hook echoes. *Electron. J. Severe Storms Meteor.*, **6** (5), http://www.ejssm.org/ojs/index.php/ejssm/article/view/93/65.

——, and A. V. Ryzhkov, 2007: Polarimetric characteristics of tornadic and nontornadic supercell thunderstorms. *33rd Conf. on Radar Meteorology,* Cairns, Queensland, Australia, Amer. Meteor. Soc., P10.1, https://ams.confex.com/ams/33Radar/techprogram/paper_122882.htm.

——, and ——, 2008a: Polarimetric signatures in supercell thunderstorms. *J. Appl. Meteor. Climatol.*, **47**, 1940–1961, https://doi.org/10.1175/2007JAMC1874.1.

——, and ——, 2008b: Microphysical differences between tornadic and nontornadic supercell rear-flank downdrafts revealed by dual-polarization radar measurements. *24th Conf. on Severe Local Storms*, Savannah, GA, Amer. Meteor. Soc., 3B.4, https://ams.confex.com/ams/24SLS/techprogram/paper_141912.htm.

——, and ——, 2009: Storm-relative helicity revealed from polarimetric radar measurements. *J. Atmos. Sci.*, **66**, 667–685, https://doi.org/10.1175/2008JAS2815.1.

——, ——, V. M. Melnikov, and T. J. Schuur, 2010: Rapid-scan super-resolution observations of a cyclic supercell with a dual-polarization WSR-88D. *Mon. Wea. Rev.*, **138**, 3762–3786, https://doi.org/10.1175/2010MWR3322.1.

——, A. P. Khain, N. Benmoshe, E. Ilotoviz, A. V. Ryzhkov, and V. T. J. Phillips, 2014: The anatomy and physics of Z_{DR} columns: Investigating a polarimetric radar signature with a spectral bin microphysical model. *J. Appl. Meteor. Climatol.*, **53**, 1820–1843, https://doi.org/10.1175/JAMC-D-13-0354.1.

——, Z. J. Lebo, and H. C. Morrison, 2015: On the mechanisms of rain formation in an idealized supercell storm. *Mon. Wea. Rev.*, **143**, 2754–2773, https://doi.org/10.1175/MWR-D-14-00402.1.

Loeffler, S. D., and M. R. Kumjian, 2018: Quantifying the separation of enhanced Z_{DR} and K_{DP} regions in nonsupercell tornadic storms. *Wea. Forecasting*, **33**, 1143–1157, https://doi.org/10.1175/WAF-D-18-0011.1.

Markowski, P. M., 2002: Hook echoes and rear-flank downdrafts: A review. *Mon. Wea. Rev.*, **130**, 852–876, https://doi.org/10.1175/1520-0493(2002)130<0852:HEARFD>2.0.CO;2.

——, J. M. Straka, and E. N. Rasmussen, 2002: Direct surface thermodynamic observations within the rear-flank downdrafts of nontornadic and tornadic supercells. *Mon. Wea. Rev.*, **130**, 1692–1721, https://doi.org/10.1175/1520-0493(2002)130<1692:DSTOWT>2.0.CO;2.

Mercer, A. E., C. M. Shafer, C. A. Doswell III, L. M. Leslie, and M. B. Richman, 2009: Objective classification of tornadic and nontornadic severe weather outbreaks. *Mon. Wea. Rev.*, **137**, 4355–4368, https://doi.org/10.1175/2009MWR2897.1.

Palmer, R. D., and Coauthors, 2011: Observations of the 10 May 2010 tornado outbreak using OU-PRIME: Potential for new science with high-resolution polarimetric radar. *Bull. Amer. Meteor. Soc.*, **92**, 871–891, https://doi.org/10.1175/2011BAMS3125.1.

Park, H., A. V. Ryzhkov, D. S. Zrnić, and K.-E. Kim, 2009: The hydrometeor classification algorithm for the polarimetric WSR-88D: Description and application to an MCS. *Wea. Forecasting*, **24**, 730–748, https://doi.org/10.1175/2008WAF2222205.1.

Parker, M. D., 2014: Composite VORTEX2 supercell environments from near-storm soundings. *Mon. Wea. Rev.*, **142**, 508–529, https://doi.org/10.1175/MWR-D-13-00167.1.

Picca, J., and A. Ryzhkov, 2012: A dual-wavelength polarimetric analysis of the 16 May 2010 Oklahoma City extreme hailstorm. *Mon. Wea. Rev.*, **140**, 1385–1403, https://doi.org/10.1175/MWR-D-11-00112.1.

Rasmussen, E. N., 2003: Refined supercell and tornado forecast parameters. *Wea. Forecasting*, **18**, 530–535, https://doi.org/10.1175/1520-0434(2003)18<530:RSATFP>2.0.CO;2.

——, and D. O. Blanchard, 1998: A baseline climatology of sounding-derived supercell and tornado forecast parameters. *Wea. Forecasting*, **13**, 1148–1164, https://doi.org/10.1175/1520-0434(1998)013<1148:ABCOSD>2.0.CO;2.

Romine, G. S., D. W. Burgess, and R. B. Wilhelmson, 2008: A dual-polarization-radar-based assessment of the 8 May 2003 Oklahoma City area tornadic supercell. *Mon. Wea. Rev.*, **136**, 2849–2870, https://doi.org/10.1175/2008MWR2330.1.

Ryzhkov, A., D. Zrnić, J. Krause, M. Kumjian, and S. Ganson, 2010: Discrimination between large and small hail, final report. NOAA/NSSL Rep., 18 pp., https://www.nssl.noaa.gov/publications/wsr88d_reports/FINAL_HailSize.doc.

Snyder, J. C., A. V. Ryzhkov, M. R. Kumjian, A. P. Khain, and J. Picca, 2015: A Z_{DR} column detection algorithm to examine convective storm updrafts. *Wea. Forecasting*, **30**, 1819–1844, https://doi.org/10.1175/WAF-D-15-0068.1.

Stensrud, D. J., J. V. Cortinas Jr., and H. E. Brooks, 1997: Discriminating between tornadic and nontornadic thunderstorms using mesoscale model output. *Wea. Forecasting*, **12**, 613–632, https://doi.org/10.1175/1520-0434(1997)012<0613:DBTANT>2.0.CO;2.

Stout, G. E., and F. A. Huff, 1953: Radar records Illinois tornadogenesis. *Bull. Amer. Meteor. Soc.*, **34**, 281–284.

Straka, J. M., D. S. Zrnić, and A. V. Ryzhkov, 2000: Bulk hydrometeor classification and quantification using polarimetric radar data: Synthesis of relations. *J. Appl. Meteor.*, **39**, 1341–1372, https://doi.org/10.1175/1520-0450(2000)039<1341:BHCAQU>2.0.CO;2.

Tanamachi, R. L., and P. L. Heinselman, 2016: Rapid-scan, polarimetric observations of central Oklahoma severe storms on 31 May 2013. *Wea. Forecasting*, **31**, 19–42, https://doi.org/10.1175/WAF-D-15-0111.1.

——, H. B. Bluestein, M. Xue, W.-C. Lee, K. A. Orzel, S. J. Frasier, and R. M. Wakimoto, 2013: Near-surface vortex structure in a tornado and in a sub-tornado-strength convective-storm vortex observed by a mobile, W-band radar during VORTEX2. *Mon. Wea. Rev.*, **141**, 3661–3690, https://doi.org/10.1175/MWR-D-12-00331.1.

Taszarek, M., H. E. Brooks, and B. Czernecki, 2017: Sounding-derived parameters associated with convective hazards in Europe. *Mon. Wea. Rev.*, **145**, 1511–1528, https://doi.org/10.1175/MWR-D-16-0384.1.

Thompson, R. L., 1998: Eta model storm-relative winds associated with tornadic and nontornadic supercells. *Wea. Forecasting*, **13**, 125–137, https://doi.org/10.1175/1520-0434(1998)013<0125:EMSRWA>2.0.CO;2.

——, R. Edwards, J. A. Hart, K. L. Elmore, and P. Markowski, 2003: Close proximity soundings within supercell environments obtained from the Rapid Update Cycle. *Wea. Forecasting*, **18**, 1243–1261, https://doi.org/10.1175/1520-0434(2003)018<1243:CPSWSE>2.0.CO;2.

——, C. M. Mead, and R. Edwards, 2007: Effective storm-relative helicity and bulk shear in supercell thunderstorm environments. *Wea. Forecasting*, **22**, 102–115, https://doi.org/10.1175/WAF969.1.

Tochimoto, E., and H. Niino, 2016: Structural and environmental characteristics of extratropical cyclones that cause tornado outbreaks in the warm sector: A composite study. *Mon. Wea. Rev.*, **144**, 945–969, https://doi.org/10.1175/MWR-D-15-0015.1.

Trapp, R. J., G. R. Marion, and S. W. Nesbitt, 2017: The regulation of tornado intensity by updraft width. *J. Atmos. Sci.*, **74**, 4199–4211, https://doi.org/10.1175/JAS-D-16-0331.1.

Van Den Broeke, M. S., 2016: Polarimetric variability of classic supercell storms as a function of environment. *J. Appl. Meteor. Climatol.*, **55**, 1907–1925, https://doi.org/10.1175/JAMC-D-15-0346.1.

——, 2017: Polarimetric radar metrics related to tornado life cycles and intensity in supercell storms. *Mon. Wea. Rev.*, **145**, 3671–3686, https://doi.org/10.1175/MWR-D-16-0453.1.

——, J. M. Straka, and E. N. Rasmussen, 2008: Polarimetric radar observations at low levels during tornado life cycles in a small sample of classic Southern Plains supercells. *J. Appl. Meteor. Climatol.*, **47**, 1232–1247, https://doi.org/10.1175/2007JAMC1714.1.

Wasserstein, R. L., and N. A. Lazar, 2016: The ASA's statement on *p*-values: Context, process, and purpose. *Amer. Stat.*, **70**, 129–133, https://doi.org/10.1080/00031305.2016.1154108.